Journal of Solid State Electrochemistry
https://doi.org/10.1007/s10008-024-05886-7

ORIGINAL PAPER

Enhanced capacity of all-solid-state battery comprising $LiNbO_3$-coated $Li(Ni_{0.8}Co_{0.1}Mn_{0.1})O_2$ Cathode, $Li_{5.4}(PS_4)(S_{0.4}Cl_{1.0}Br_{0.6})$ solid electrolyte and lithium metal anode

Naoya Masuda[1,2] · Kiyoshi Kobayashi[3] · Futoshi Utsuno[1] · Naoaki Kuwata[2,4]

Received: 6 February 2024 / Revised: 1 April 2024 / Accepted: 1 April 2024

Abstract

All-solid-state lithium-ion batteries are a promising next-generation technology because they have higher energy densities than their liquid-electrolyte counterparts. Halogen-rich argyrodite, specifically $Li_{5.4}(PS_4)(S_{0.4}Cl_{1.0}Br_{0.6})$, was recently shown to have higher ionic conductivities compared with those of other argyrodite-like sulfides. Although the $Li_{5.4}(PS_4)(S_{0.4}Cl_{1.0}Br_{0.6})$ in Li | $Li_{5.4}(PS_4)(S_{0.4}Cl_{1.0}Br_{0.6})$ | $Li(Ni_{0.8}Co_{0.1}Mn_{0.1})O_2$–$Li_{5.4}(PS_4)(S_{0.4}Cl_{1.0}Br_{0.6})$ batteries have shown good electrochemical stability, the low discharge capacity limits the application of the battery. In continuation, this study examined the potential of a carbon additive for altering the electronic conductivity of the cathode and enhancing the capacity of Li | $Li_{5.4}(PS_4)(S_{0.4}Cl_{1.0}Br_{0.6})$ | $Li(Ni_{0.8}Co_{0.1}Mn_{0.1})O_2$–$Li_{5.4}(PS_4)(S_{0.4}Cl_{1.0}Br_{0.6})$ batteries. After a 50-cycle charge/discharge, the carbon additive (0.1 C) enhanced the discharge capacity from 3.1 to 167 mAh/g, resulted in a capacity retention rate and coulombic efficiency of 95.4% and 99.9% when using 0.1 C and 0.5 C, respectively, and increased the resistance of the battery from 53 to 56 Ω. Therefore, the all-solid-state battery employing high-ion-conductive $Li_{5.4}(PS_4)(S_{0.4}Cl_{1.0}Br_{0.6})$ and a carbon-modified cathode showed improved capacity. This study provides a proven framework for developing all-solid-state batteries employing halogen-rich argyrodite ($Li_{7-\alpha}(PS_4)(S_{2-\alpha}X_\alpha)$; $\alpha > 1$) with enhanced ionic conductivities.

Keywords All-solid-state battery · Argyrodite · Halogen-rich · High capacity · Solid electrolyte

Introduction

Various high-performance lithium-ion rechargeable batteries, such as all-solid-state batteries, have been developed to address the demand for technological development under the challenges of climate change [1] and realize a sustainable carbon-neutral society [2–4]. The performance of all-solid-state batteries mostly depends on the electrochemical properties and lithium-ion conductivity of the electrolyte [5]. Although conventional all-solid-state lithium-ion batteries have low-rate capabilities and energy densities, recent studies have demonstrated that lithium–phosphorus–sulfide solid electrolytes (SE) show improved ionic conductivity [6–8] and may be easily integrated into battery production because of their mechanical softness [9] and facile processing [10].

Among the phosphorus sulfides, we have discovered various $Li_{7-\alpha}PS_{6-\alpha}X_\alpha$ (X = Cl, Br, I) argyrodites that exhibit high ionic conductivities [11–17], denoted as $Li_{7-\alpha}(PS_4)(S_{2-\alpha}X_\alpha)$ [18]. In a $Li_{7-x-y}(PS_4)(S_{2-x-y}Cl_xBr_y)$ system [18], $Li_{5.4}(PS_4)(S_{0.4}Cl_{1.0}Br_{0.6})$ showed excellent electrochemical stability in Li | $Li_{5.4}(PS_4)(S_{0.4}Cl_{1.0}Br_{0.6})$ | $Li(Ni_{0.8}Co_{0.1}Mn_{0.1})O_2$–$Li_{5.4}(PS_4)(S_{0.4}Cl_{1.0}Br_{0.6})$ batteries. Nevertheless, the discharge capacity of this battery (140 mAh/g) was still lower than those of other all-solid-state batteries (> 140 mAh/g) [19].

To explain the low discharge capacity, we measured the electronic and ionic conductivities of cathode mixtures. Changing the amount of cathode active material from 70 to 90 wt% increased the electronic conductivity of the cathode

✉ Naoya Masuda
naoya.masuda.3920@idemitsu.com

1 Research Center for Battery Materials, Idemitsu Kosan Co., Ltd, Sodegaura, Chiba 299-0293, Japan

2 Graduate School of Chemical Sciences and Engineering, Hokkaido University, Sapporo, Hokkaido 060-8628, Japan

3 Research Center for Electronic and Optical Materials, National Institute for Materials Science, 1-2-1, Sengen, Tsukuba, Ibaraki 305-0047, Japan

4 Center for Green Research on Energy and Environmental Materials, National Institute for Materials Science, 1-1 Namiki, Tsukuba, Ibaraki 305-0044, Japan

Published online: 04 April 2024

mixture, but reduced its ionic conductivity. Unfortunately, both high electronic and lithium-ion conductivities are necessary for generating an effective composite cathode. In addition, much predomination of electronic conductivity contributes to the discharge capacity [19].

Several studies have attempted to enhance the capacity of various sulfide solid electrolytes using a carbon additive (CA) to increase the electronic conductivity of the cathode [20–42]. The discharge capacity of the Li | β-Li_3PS_4 | $Li(Ni_{0.6}Co_{0.2}Mn_{0.2})O_2$–β-$Li_3PS_4$ battery increased with a CA-modified cathode. However, the capacity retention rate was ~ 85% after 50 cycles [23]. Similarly, the retention rate of the In-Li | $Li_{6.0}(PS_4)(S_{1.0}Cl_{1.0})$ | $Li(Ni_{0.6}Co_{0.2}Mn_{0.2})O_2$–$Li_{6.0}(PS_4)(S_{1.0}Cl_{1.0})$ battery was 79% after 50 cycles [42]. With a CA, the capacity decreased with repeated cycles, although the initial capacity was high [23]. The decreased capacity after cycling was likely related to a decomposition reaction of SE, although the mechanism remains unclear [43, 44]. However, it is unclear whether an all-solid-state battery with a CA-modified cathode can maintain a consistent capacity after cycling.

We hypothesized that a CA-modified cathode would enhance the capacity of an all-solid-state battery using a high ion-conductive $Li_{5.4}(PS_4)(S_{0.4}Cl_{1.0}Br_{0.6})$ solid electrolyte. We previously showed that batteries with a cathode mixture consisting of 70 wt% active material and 30 wt% $Li_{5.4}(PS_4)(S_{0.4}Cl_{1.0}Br_{0.6})$ had the lowest capacity [19]; however, the capacity of the battery may be rescued by adding CA to increase the electronic conductivity of the cathode mixture [19]. Unfortunately, the effects of CA cathode modifications in all-solid-state $Li_{5.4}(PS_4)(S_{0.4}Cl_{1.0}Br_{0.6})$ batteries are unclear. To increase the battery capacity, the cathode mixture should preferably have a high active material ratio. However, we selected 70 wt% active material and 30 wt% $Li_{5.4}(PS_4)(S_{0.4}Cl_{1.0}Br_{0.6})$ to investigate the effect of electronic conductivity on capacity during cycling. We measured the changes in the discharge capacity and capacity retention rates of the Li | $Li_{5.4}(PS_4)(S_{0.4}Cl_{1.0}Br_{0.6})$ | $Li(Ni_{0.8}Co_{0.1}Mn_{0.1})O_2$–$Li_{5.4}(PS_4)(S_{0.4}Cl_{1.0}Br_{0.6})$–CA battery using cycling tests, followed by impedance analysis to evaluate the battery resistance during cycling.

Methods

Synthesis of solid electrolyte and cathode mixture

$Li_{5.4}(PS_4)(S_{0.4}Cl_{0.1}Br_{0.6})$ powder and $LiNbO_3$-coated $Li(Ni_{0.8}Co_{0.1}Mn_{0.1})O_2$ were synthesized and the thickness of the coated layer (4.2 nm) was calculated, as we have previously described [18, 19]. Mixed cathode powders were prepared using $LiNbO_3$-coated $Li(Ni_{0.8}Co_{0.1}Mn_{0.1})O_2$, $Li_{5.4}(PS_4)(S_{0.4}Cl_{1.0}Br_{0.6})$, and CA (Li100, Denka) in weight ratios of 70:30:0 (0 vol%), 70:30:3.4 (5 vol%), 70:30:7.2 (10 vol%), and 70:30:21.5 (25 vol%), respectively. CA made from acetylene black was selected in this study because it has previously been reported to maintain a high-capacity retention rate even after cycling [20]. The densities for $Li(Ni_{0.8}Co_{0.1}Mn_{0.1})O_2$ and $Li_{5.4}(PS_4)(S_{0.4}Cl_{1.0}Br_{0.6})$ were selected as previously described [19] and the CA load was 2.16 g/cm^3 [45]. The volume ratios were calculated from these densities and weight ratios. Volume ratio is used to describe the percolation of ions and electrons within a three-dimensional composite cathode [46]. The cathode mixtures were placed in a ZrO_2 pot (45 ml) containing a ZrO_2 ball (2.0 mm diameter; 34 g) in an argon-filled glovebox for dry ball-milling. The mixing condition was the same as in our previous study [19].

All-solid-state battery fabrication and electrochemical measurements

We fabricated a battery with a Li | $Li_{5.4}(PS_4)(S_{0.4}Cl_{1.0}Br_{0.6})$ | $Li(Ni_{0.8}Co_{0.1}Mn_{0.1})O_2$–$Li_{5.4}(PS_4)(S_{0.4}Cl_{1.0}Br_{0.6})$–CA structure. The total amount of cathode active material was 18 mg. Lithium foil (10 mm diameter, 0.2 mm thickness; Honjo Metal, Osaka, Japan) was used as the anode. The solid electrolyte (100 mg) was pressed into 10-mm-diameter pellets at 300 MPa. The cathode mixtures were pressed into 10-mm-diameter pellets at 600 MPa to form a cathode electrode layer. Finally, lithium metal was attached to the opposite side of the cathode and pressed at 100 MPa.

Electrochemical measurements were performed while the battery pellets were loaded at 20 MPa using a screw and torque wrench. The battery was charged and discharged between 2.5 and 4.3 V at 298 K using a potentio-galvanostat (VMP-3, Biologic, Seyssinet-Pariset, France). The atmosphere contained less than 1 ppm moisture and oxygen. The current density was fixed at 0.24 or 1.2 mA/cm^2, corresponding to 0.1 C and 0.5 C, respectively. Impedance spectra were collected using the potentio-galvanostat. The charge and discharge capacity values at the 1st, 2nd, 10th, 20th, 30th, 40th, and 50th cycles were measured at 0.1 C. The values at all other cycles were measured at 0.5 C to accelerate the capacity degradation. Impedance spectra were collected at the 1st, 10th, 20th, 30th, 40th, and 50th cycles under a state of charge (SOC) of 0%, 50%, and 100%. Before conducting the impedance measurements, the charge and discharge operations were stopped for 5 min. Impedance spectra were measured for the open-cell state with a voltage amplitude of 10 mV over a frequency range of 10^6 to 0.01 Hz at 298 K. All measurements were conducted under 1 ppm of moisture and oxygen. For an all-solid-state battery comprising a sulfide solid electrolyte, 300 to 600 MPa can be applied to manufacture the pellet and 10 to 70 MPa during cycling

[18, 19, 47–49]. Impedance spectra were fitted using Zmeam software (Zmeam_v109002) [50].

Ionic and electronic conductivity measurements of cathode mixtures

The ionic and electronic conductivities of the cathode mixtures were measured as previously described [19]. The ionic conductivities of the cathode mixtures were measured using an electron-blocking cell with a Li | $Li_{5.4}(PS_4)(S_{0.4}Cl_{1.0}Br_{0.6})$ | $Li(Ni_{0.8}Co_{0.1}Mn_{0.1})O_2$–$Li_{5.4}(PS_4)(S_{0.4}Cl_{1.0}Br_{0.6})$–CA | $Li_{5.4}(PS_4)(S_{0.4}Cl_{1.0}Br_{0.6})$ | Li structure. Cathode mixtures (total weight: 200 mg) sandwiched with 50 mg of $Li_{5.4}(PS_4)(S_{0.4}Cl_{1.0}Br_{0.6})$ from both sides were pressed into 10-mm-diameter pellets at 600 MPa. Subsequently, Li foil (10 mm φ, thickness: 0.2 mm; Honjo Metal) was applied on both ends and pressed at 100 MPa. Constant voltages (E_{app_i}) of 10, 20, 30, 40, and 50 mV were applied for 2 h. The resistance of the electron-blocking cell was calculated from the slope between E_{app_i} and current using the current and voltage values obtained after 2 h. The electron-blocking cell resistance includes the solid electrolyte and mixture resistances. The resistance of the solid electrolyte and cell length of $Li_{5.4}(PS_4)(S_{0.4}Cl_{1.0}Br_{0.6})$ (equivalent to 16.2 Ω and 7.4×10^{-2} cm at 100 mg, respectively) were calculated [18] and subtracted from the electron-blocking cell resistance. The ionic conductivity was calculated using the surface area (0.785 cm^2), subtracted resistance, and cell length. The measurements were performed while the electron-blocking cell was compressed at 20 MPa using a screw and torque wrench in an atmosphere with 1 ppm moisture and oxygen.

The electronic conductivity of the cathode composites was measured using an ion-blocking electrode of stainless steel (SUS) | $Li(Ni_{0.8}Co_{0.1}Mn_{0.1})O_2$–$Li_{5.4}(PS_4)(S_{0.4}Cl_{1.0}Br_{0.6})$–CA | SUS. The ion-blocking electrode (total weight: 200 mg) was pressed into 10-mm-diameter pellets under 600 MPa. Thereafter, constant voltages (E_{app_e}) of 10, 20, 30, 40, and 50 mV were applied to the electrode pellets for 2 h, and the resistance of the composite was calculated from the slope between E_{app_e} and current. This calculation does not require correction of the solid electrolyte resistance. The measurements were performed while the electrode pellets were compressed at 20 MPa using a screw and torque wrench in an atmosphere with 1 ppm moisture and oxygen.

Results and discussion

Charge and discharge capacities of Li | $Li_{5.4}(PS_4)(S_{0.4}Cl_{1.0}Br_{0.6})$ | $Li(Ni_{0.8}Co_{0.1}Mn_{0.1})O_2$–$Li_{5.4}(PS_4)(S_{0.4}Cl_{1.0}Br_{0.6})$-CA batteries

In our previous study, the battery using $LiNbO_3$-coated $Li(Ni_{0.8}Co_{0.1}Mn_{0.1})O_2$ and $Li_{5.4}(PS_4)(S_{0.4}Cl_{1.0}Br_{0.6})$ in weight ratios of 70:30 without CA exhibited the lowest discharge capacity among the batteries comprising different ratios of $Li(Ni_{0.8}Co_{0.1}Mn_{0.1})O_2$ and $Li_{5.4}(PS_4)(S_{0.4}Cl_{1.0}Br_{0.6})$ [19]. The discharge capacity and capacity retention rate of the battery using 70:30 $LiNbO_3$-coated $Li(Ni_{0.8}Co_{0.1}Mn_{0.1})O_2$ and $Li_{5.4}(PS_4)(S_{0.4}Cl_{1.0}Br_{0.6})$ after 50 cycles were 3.1 mAh/g and 99.1%, respectively. Compared with that when using 0 vol% CA in the cathode mixture [$LiNbO_3$-coated $Li(Ni_{0.8}Co_{0.1}Mn_{0.1})O_2$ and $Li_{5.4}(PS_4)(S_{0.4}Cl_{1.0}Br_{0.6})$ in weight ratios of 70:30], the discharge capacity increased from 3.1 to 167 mAh/g after 50 cycles when using 5 vol% (Fig. 1a). The capacity retention rate and coulombic efficiency after 50 charge/discharge cycles were 95.4% and 99.9% when using 0.1 C and 0.5 C, respectively. This represents a much higher capacity retention rate compared with that of the In-Li | $Li_{6.0}(PS_4)$

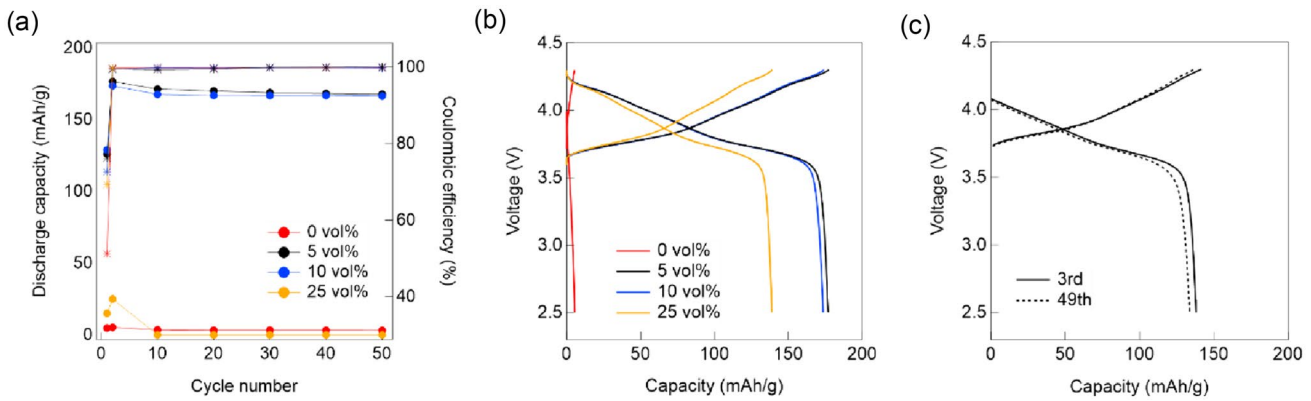

Fig. 1 **a** Cycling durability (filled circles) and coulombic efficiency (asterisks) of the all-solid-state battery using (red) 0 vol%, (black) 5 vol%, (blue) 10 vol%, and (orange) 25 vol% cathode mixtures measured at 0.1 C. **b** Charge/discharge curve of 2nd cycle at 0.1 C. The red, black, blue, and orange lines represent 0 vol%, 5 vol%, 10 vol%, and 25 vol%, respectively. **c** Capacity curve of all-solid-state battery using 5 vol% cathode at 3rd and 49th cycle charged/discharged at 0.5 C

$(S_{1.0}Cl_{1.0})$ | $Li(Ni_{0.6}Co_{0.2}Mn_{0.2})O_2$–$Li_{6.0}(PS_4)(S_{1.0}Cl_{1.0})$ battery [42] after 50 cycles (79%). However, the discharge capacity decreased when the amount of CA exceeded 5 vol%. The discharge capacity of the battery using 25 vol% was 25 mAh/g at most in the initial cycle and the battery suddenly short-circuited after 6 cycles. The first explanation for this phenomenon is that decomposed products formed at the SE/CA interface, such as the decomposition of solid electrolyte observed by cyclic voltammogram in the Li | β-Li_3PS_4 | β-Li_3PS_4-CA configuration [43]. The bonding of terminal sulfur such as PS_4 tetrahedra in β-Li_3PS_4 was experimentally confirmed to be decomposed into bridged sulfur compounds (-S-) above 3.5 V [43, 44]. This indicated that PS_4 tetrahedra containing solid electrolyte decomposed at high voltage. In our previous study, $Li_{5.4}(PS_4)(S_{0.4}Cl_{1.0}Br_{0.6})$ was stable above 10 V without CA. This suggests that an increased probability of reaction between the CA and $Li_{5.4}(PS_4)(S_{0.4}Cl_{1.0}Br_{0.6})$ exists in batteries using the 25 vol% cathode. Notably, 10 vol% corresponded to a high discharge capacity, almost equivalent to that at 5 vol%. This suggests that $Li_{5.4}(PS_4)(S_{0.4}Cl_{1.0}Br_{0.6})$ is stable and its decomposition is negligible in the 10 vol% cathode. The second explanation is that decomposed products were formed at the $Li(Ni_{0.8}Co_{0.1}Mn_{0.1})O_2/Li_{5.4}(PS_4)(S_{0.4}Cl_{1.0}Br_{0.6})$ interface. We previously reported amorphous impurities generated at the $Li(Ni_{0.8}Co_{0.1}Mn_{0.1})O_2/Li_{5.4}(PS_4)(S_{0.4}Cl_{1.0}Br_{0.6})$ interface during cycling, which increased impedance. Because we used a similar composition of cathode active material and solid electrolyte, we presumed that amorphous impurities formed in systems with high CA contents [19]. A third explanation is that impurities were generated at the $Li(Ni_{0.8}Co_{0.1}Mn_{0.1})O_2$/CA interface, though this requires validation [23]. Consequently, we hypothesized that the short circuit in 25 vol% CA batteries was due to the decomposition reactions at the $Li_{5.4}(PS_4)(S_{0.4}Cl_{1.0}Br_{0.6})$/CA and $Li(Ni_{0.8}Co_{0.1}Mn_{0.1})O_2/Li_{5.4}(PS_4)(S_{0.4}Cl_{1.0}Br_{0.6})$ interfaces.

We previously measured the electronic and ionic conductivities of cathode mixtures without CA and found that changing the cathode active material content from 70 to 90 wt% promoted electronic conductivity while reducing ionic conductivity. Because electronic conductivity changed more drastically than ionic conductivity, it is likely that electronic conductivity was the key factor affecting discharge capacity [19]. We adjusted the amount of CA (from 0 to 25 vol%) in the battery comprising 70:30 $LiNbO_3$-coated $Li(Ni_{0.8}Co_{0.1}Mn_{0.1})O_2$ and $Li_{5.4}(PS_4)(S_{0.4}Cl_{1.0}Br_{0.6})$ and found that the electronic conductivities of the cathode mixtures increased greatly from 2.6×10^{-8} to 1.1 S/cm with a CA modification (Fig. 2).

The lithium-ion conductivity between 0 and 25 vol% was about 2.9×10^{8} times smaller than the electronic conductivity. The small degree of change in ionic conductivity was likely due to the weak influence on $Li_{5.4}(PS_4)(S_{0.4}Cl_{1.0}Br_{0.6})$ conduction path structure [18, 19].

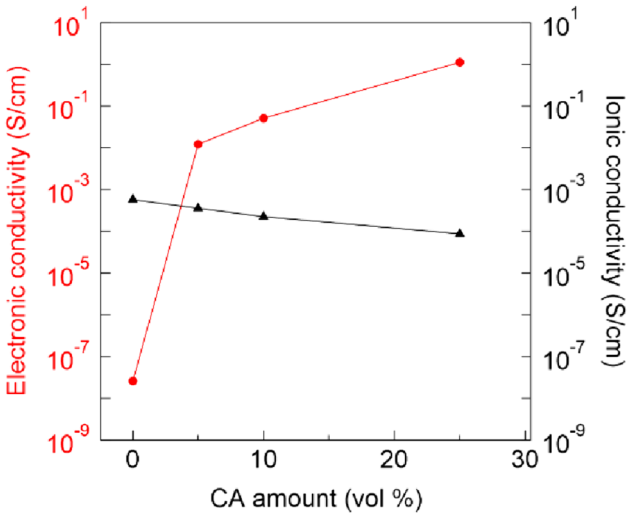

Fig. 2 Ionic and electronic conductivities of the cathode mixture with increasing amounts of CA

The all-solid-state battery using the $Li(Ni_{0.8}Co_{0.1}Mn_{1.0})O_2$ and β-Li_3PS_4 cathode (ionic conductivity: ~ 0.1 mS/cm) mixture showed a high capacity (120 mAh/g) without CA [51–54]. In contrast, we measured 3.1 mAh/g after 50 cycles in our all-solid-state battery using a high-ion-conductive solid electrolyte, $Li_{5.4}(PS_4)(S_{0.4}Cl_{1.0}Br_{0.6})$ (12 mS/cm), without a CA-modified cathode. Battery capacity may decrease even if the ionic or electronic conductivity of the cathode is high [55, 56], likely because the charge/discharge reaction caused by charge transfer involves both lithium-ion and electron conduction in the electrode [55, 56]. These results emphasize the importance of the electronic conductivity of the cathode mixture when optimizing battery capacity in a system incorporating a high-ion-conductive $Li_{5.4}(PS_4)(S_{0.4}Cl_{1.0}Br_{0.6})$ solid electrolyte. This high ionic conductivity is also attributed to the high discharge capacity at 0.5 C [55, 56]. Compared with the discharge capacity (< 10 mAh/g) of the Li | β-Li_3PS_4 | $Li(Ni_{0.8}Co_{0.1}Mn_{1.0})O_2$–β-$Li_3PS_4$ battery [51], the all-solid-state battery with 5 vol% CA recorded 137 mAh/g and 134 mAh/g at the 3rd and 49th cycles, respectively (Fig. 1c).

Impedance spectra of Li | $Li_{5.4}(PS_4)(S_{0.4}Cl_{1.0}Br_{0.6})$ | $Li(Ni_{0.8}Co_{0.1}Mn_{0.1})O_2$–$Li_{5.4}(PS_4)(S_{0.4}Cl_{1.0}Br_{0.6})$-CA batteries

Impedance spectra are shown in Fig. 3a–d. We previously reported that $Li_{5.4}(PS_4)(S_{0.4}Cl_{1.0}Br_{0.6})$ showed constant resistance at a high frequency due to its high chemical stability. However, we could not separate the bulk and grain boundary due to the measurement frequency region and

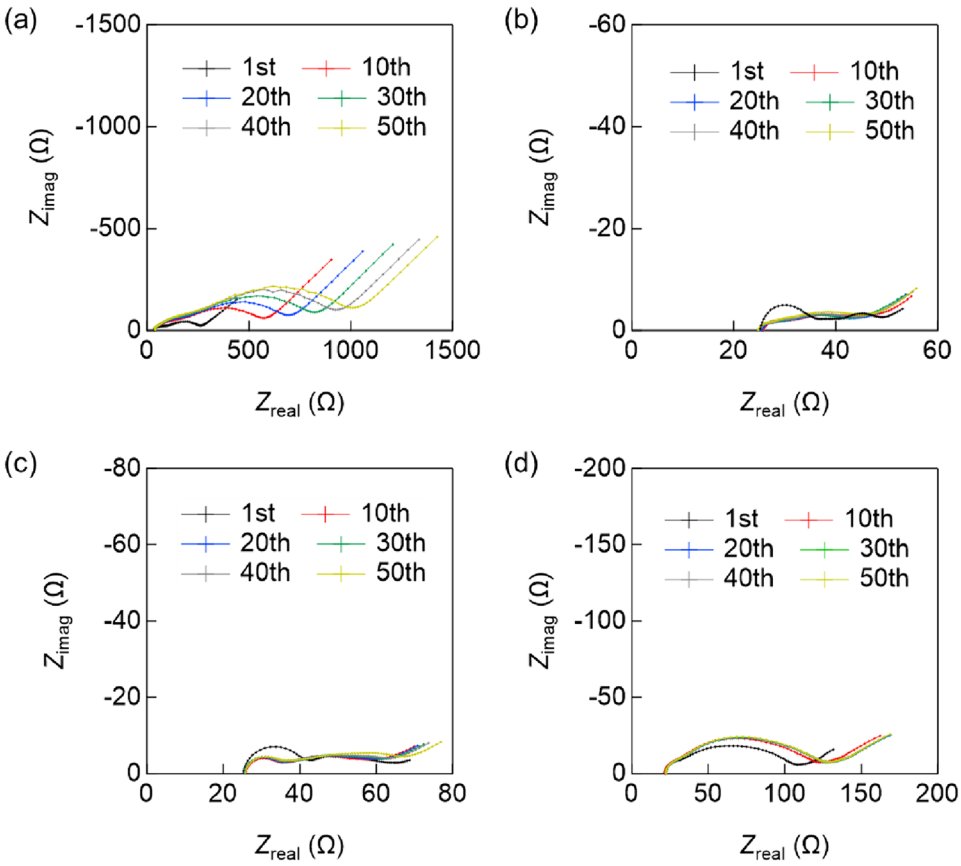

Fig. 3 Impedance spectra of battery using **a** 0 vol%, **b** 5 vol%, **c** 10 vol%, and **d** 25 vol% CA, respectively, after 50 cycles

temperature [18.19], as previously reported [57]. In the present study, we found that $Li_{5.4}(PS_4)(S_{0.4}Cl_{1.0}Br_{0.6})$ was stable even at up to 10 vol% CA in the all-solid-state battery comprising Li | $Li_{5.4}(PS_4)(S_{0.4}Cl_{1.0}Br_{0.6})$ | $Li(Ni_{0.8}Co_{0.1}Mn_{0.1})O_2$–$Li_{5.4}(PS_4)(S_{0.4}Cl_{1.0}Br_{0.6})$-CA. Tables S1–S4 show the impedance estimates calculated using an equivalent circuit model (Fig. 4a–d).

In the battery using the highest capacity 5-vol% CA cathode mixture, resistance increased from 53 to 56 Ω during 50 cycles. We previously reported that the impedance of a high-capacity battery increased from 85 to 135 Ω during 50 cycles [19], which was presumed to be due to the formation of amorphous impurities. We also found that $Li_{5.4}(PS_4)(S_{0.4}Cl_{1.0}Br_{0.6})$ was stable against Li metal [18]. $Li_{5.4}(PS_4)(S_{0.4}Cl_{1.0}Br_{0.6})$ is electrochemically stable during cycling because the calculated resistances at high frequency using an equivalent circuit model remained unchanged during 50 cycles (Fig. 4a–d), Tables S1–S4). Previous results indicated that the battery using the 5 vol% CA cathode mixture was highly stable after 50 cycles.

Assuming a homogeneous electrode, Warburg impedance can be measured at low frequencies as a finite length of material diffusion [58, 59]. In all-solid-state batteries, the Warburg coefficient reflects the ease with which lithium-ion diffuses within the electrode [60]. Warburg impedance did not appear when measuring impedance in a Li | SE | Li cell configuration after flowing a current equivalent to 50% of SOC (Fig. S1). When the Warburg coefficients were compared, it was observed that lithium-ion tended to diffuse more easily into positive electrodes incorporating 5 and 10 vol% CA-modified cathodes. In contrast, Li diffusion was limited at 0 and 25 vol% (Tables S1–S4), reflecting the change in capacity. Although Warburg impedance in this study is assumed to be homogeneous in cathodes, actual cathodes are composites of cathode active materials, solid electrolytes, and CA. In the case of a composite structure, macroscopic Li diffusion would be strongly influenced by its morphology [58, 59]. However, we did not analyze morphology-dependent changes in Li diffusion during cycling because the pellets containing CA were too brittle to be observed via scanning electron microscopy (Fig. S2). Therefore, clarifying the relationship between cathode performance, impedance spectra, and cathode morphology will be the next step in manufacturing high-performance composite cathodes.

CA modification was previously reported to increase capacity by increasing cathode active material [$Li(Ni_{0.6}Co_{0.6}Mn_{0.6})O_2$] utilization rates. However, as the utilization rate increased, deterioration reactions at the β-Li_3PS_4/CA interface progressed, causing a decrease in capacity during cycling [23].

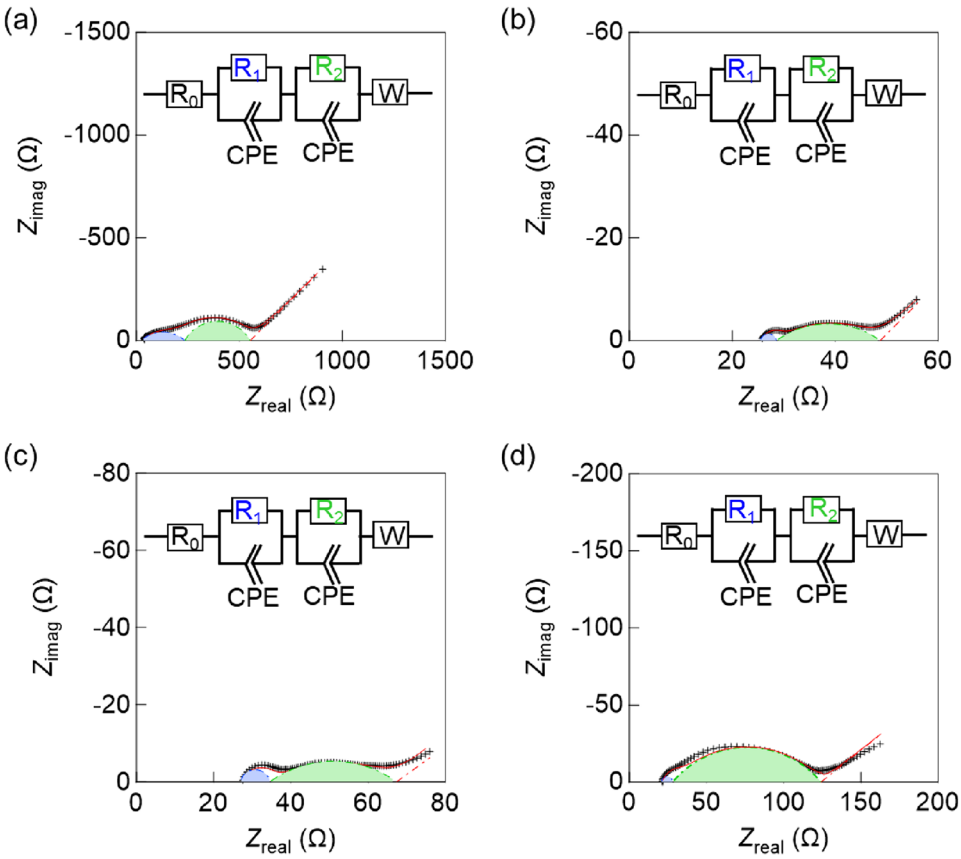

Fig. 4 Impedance spectra at the 10th cycle using **a** 0 vol%, **b** 5 vol%, **c** 10 vol%, and **d** 25 vol% CA cathode mixture fitted using the inset equivalent circuit models, as previously reported [19]. The spectra were fitted using Zmeam software [50]

In this study, the utilization rate of $Li(Ni_{0.8}Co_{0.1}Mn_{0.1})O_2$ increased by adding CA, capacity decrease during cycling was small, and there was little increase in impedance, indicating limited decomposition reactions at the $Li_{5.4}(PS_4)(S_{0.4}Cl_{1.0}Br_{0.6})$/CA interface.

Conclusion

This study evaluated the discharge capacity of an all-solid-state battery with a Li | $Li_{5.4}(PS_4)(S_{0.4}Cl_{1.0}Br_{0.6})$ | $Li(Ni_{0.8}Co_{0.1}Mn_{0.1})O_2$–$Li_{5.4}(PS_4)(S_{0.4}Cl_{1.0}Br_{0.6})$-CA structure. In conventional all-solid-state batteries, the initial capacity was high with a CA but decreased with cycling. The CA improved the electronic conductivity of the cathode mixture and increased the discharge capacity from 3.1 to 167 mAh/g after 50 cycles. The resistance of the battery increased from 53 to 56 Ω during 50 charge/discharge cycles. These findings demonstrate that the battery capacity of an all-solid-state battery employing a high-ionic conductive $Li_{5.4}(PS_4)(S_{0.4}Cl_{1.0}Br_{0.6})$ can be increased with a CA modification that enhances the electronic conductivity of the cathode. This study presents a proven framework for developing an all-solid-state battery comprising halogen-rich argyrodite ($Li_{7-\alpha}(PS_4)(S_{2-\alpha}X_\alpha)$; $\alpha > 1$) with enhanced ionic conductivities by controlling the electronic conductivity of the cathode. We plan to further improve battery performance by elucidating the relationship between the battery performance, actual cathode structure, and impedance during cycling in a future study.

Supplementary Information The online version contains supplementary material available at https://doi.org/10.1007/s10008-024-05886-7.

Author contributions Naoya Masuda performed all syntheses, electrochemical measurements, and analyses. The paper was written by Naoya Masuda and Kiyoshi Kobayashi with input from Futoshi Utsuno and Naoaki Kuwata.

Declarations

Competing interests The authors declare no competing interests.

References

1. Jacobson MZ (2009) Review of solutions to global warming, air pollution, and energy security. Energy Environ Sci 2:148–173. https://doi.org/10.1039/B809990C
2. Hannan MA, Lipu MSH, Hussain A, Mohamed A (2017) A review of lithium-ion battery state of charge estimation and management system in electric vehicle applications: challenges

and recommendations. Renew Sustain Energy Rev 78:834–854. https://doi.org/10.1016/j.rser.2017.05.001
3. Janek J, Zeier WG (2016) A solid future for battery development. Nat Energy 1:16141. https://doi.org/10.1038/nenergy.2016.141
4. Kato Y, Hori S, Saito T, Suzuki K, Hirayama M, Mitsui A, Yonemura M, Iba H, Kanno R (2016) High-power all-solid-state batteries using sulfide superionic conductors. Nat Energy 1:16030. https://doi.org/10.1038/nenergy.2016.30
5. Boulineau S, Tarascon JM, Leriche JB, Viallet V (2013) Electrochemical properties of all-solid-state lithium secondary batteries using Li-argyrodite Li_6PS_5Cl as solid electrolyte. Solid State Ionics 242:45–48. https://doi.org/10.1016/j.ssi.2013.04.012
6. Wang P, Liu H, Patel S, Feng X, Chien P-H, Wang Y, Hu YY (2020) Fast ion conduction and its origin in $Li_{6-x}PS_{5-x}Br_{1+x}$. Chem Mater 32:3833–3840. https://doi.org/10.1021/acs.chemmater.9b05331
7. Feng X, Chien P-H, Wang Y, Patel S, Wang P, Liu H, Immediato-Scuotto M, Hu YY (2020) Enhanced ion conduction by enforcing structural disorder in Li-deficient argyrodites $Li_{6-x}PS_{5-x}Cl_{1+x}$. Energy Stor Mater 30:67–73. https://doi.org/10.1016/j.ensm.2020.04.042
8. Adeli P, Bazak JD, Park KH, Kochetkov I, Huq A, Goward GR, Nazar LF (2019) Boosting solid-state diffusivity and conductivity in lithium superionic argyrodites by halide substitution. Angew Chem Int Ed Engl 58:8681–8686. https://doi.org/10.1002/anie.201814222
9. Adeli P, Bazak JD, Huq A, Goward GR, Nazar LF (2021) Influence of aliovalent cation substitution and mechanical compression on Li-ion conductivity and diffusivity in argyrodite solid electrolytes. Chem Mater 33:146–157. https://doi.org/10.1021/acs.chemmater.0c03090
10. Suyama M, Kato A, Sakuda A, Hayashi A, Tatsumisago M (2018) Lithium dissolution/deposition behavior with Li_3PS_4-LiI electrolyte for all-solid-state batteries operating at high temperatures. Electrochim Acta 286:158–162. https://doi.org/10.1016/j.electacta.2018.07.227
11. Epp V, Gün Ö, Deiseroth HJ, Wilkening M (2013) Highly mobile ions: low-temperature NMR directly probes extremely fast Li^+ hopping in argyrodite-type Li_6PS_5Br. J Phys Chem Lett 4:2118–2123. https://doi.org/10.1021/jz401003a
12. Gautam A, Sadowski M, Ghidiu M, Minafra N, Senyshyn A, Albe K, Zeier WG (2021) Engineering the site-disorder and lithium distribution in the lithium superionic argyrodite Li_6PS_5Br. Adv Energy Mater 11:2003369. https://doi.org/10.1002/aenm.202003369
13. Patel SV, Banerjee S, Liu H, Wang P, Chien PH, Feng X, Liu J, Ong SP, Hu YY (2021) Tunable lithium-ion transport in mixed-halide argyrodites $Li_{6-x}PS_{5-x}ClBr_x$: an unusual compositional space. Chem Mater 33:1435–1443. https://doi.org/10.1021/acs.chemmater.0c04650
14. De Klerk NJJ, Rosłoń I, Wagemaker M (2016) Diffusion mechanism of Li argyrodite solid electrolytes for Li-ion batteries and prediction of optimized halogen doping: the effect of Li vacancies, halogens, and halogen disorder. Chem Mater 28:7955–7963. https://doi.org/10.1021/acs.chemmater.6b03630
15. Kraft MA, Culver SP, Calderon M, Böcher F, Krauskopf T, Senyshyn A, Dietrich C, Zevalkink A, Janek J, Zeier WG (2017) Influence of lattice polarizability on the ionic conductivity in the lithium superionic argyrodites Li_6PS_5 X (X = Cl, Br, I). J Am Chem Soc 139:10909–10918. https://doi.org/10.1021/jacs.7b06327
16. Yu C, Li Y, Li W, Adair KR, Zhao F, Willans M, Liang J, Zhao Y, Wang C, Deng S, Li R, Huang H, Lu S, Sham TK, Huang Y, Sun X (2020) Enabling ultrafast ionic conductivity in Br-based lithium argyrodite electrolytes for solid-state batteries with different anodes. Energy Stor Mater 30:238–249. https://doi.org/10.1016/j.ensm.2020.04.014
17. Subramanian Y, Rajagopal R, Ryu KS (2022) Synthesis, air stability and electrochemical investigation of lithium superionic bromine substituted argyrodite ($Li_{6-x}PS_{5-x}Cl_{1.0}Br_x$) for all-solid-state lithium batteries. J Power Sources 520:230849. https://doi.org/10.1016/j.jpowsour.2021.230849
18. Masuda N, Kobayashi K, Utsuno F, Uchikoshi T, Kuwata N (2022) Effects of halogen and sulfur mixing on lithium-ion conductivity in $Li_{7-x-y}(PS_4)(S_{2-x-y}Cl_xBr_y)$ argyrodite and mechanism for enhanced lithium conduction. J Phys Chem C 126:14067–14074. https://doi.org/10.1021/acs.jpcc.2c03780
19. Masuda N, Kobayashi K, Utsuno F, Uchikoshi T, Kuwata N (2023) Electrochemical stability of $Li_{5.4}(PS_4)(S_{0.4}Cl_{1.0}Br_{0.6})$ in an all-solid-state battery comprising $LiNbO_3$-coated $Li(Ni_{0.8}Co_{0.1}Mn_{0.1})O_2$ cathode and lithium metal anode. J Electrochem Soc 170:090529. https://doi.org/10.1149/1945-7111/acf880
20. Yubuchi S, Uematsu M, Hotehama C, Sakuda A, Hayashi A, Tatsumisago M (2019) An argyrodite sulfide-based superionic conductor synthesized by a liquid-phase technique with tetrahydrofuran and ethanol. J Mater Chem A 7:558–566. https://doi.org/10.1039/C8TA09477B
21. Park SW, Oh G, Park JW, Ha YC, Lee SM, Toon SY, Kim BG (2019) Graphitic hollow nanocarbon as a promising conducting agent for solid-state lithium batteries. Small 15:1900235. https://doi.org/10.1039/C8TA09477B
22. Wang CW, Ren FC, Zhou Y, Yan PF, Zhou XD, Zhang SJ, Liu W, Zhang WD, Zou MH, Zeng LY, Yao XY, Huang L, Li JT, Sun SG (2021) Engineering the interface between $LiCoO_2$ and $Li_{10}GeP_2S_{12}$ solid electrolytes with an ultrathin $Li_2CoTi_3O_8$ interlayer to boost the performance of all-solid-state batteries. Energy Environ Sci 14:437–450. https://doi.org/10.1039/D0EE03212C
23. Walther F, Randau S, Schneider Y, Sann J, Rohnke M, Richter FH, Zeier WG, Janek J (2020) Influence of carbon additives on the decomposition pathways in cathodes of lithium thiophosphate-based all-solid-state batteries. Chem Mater 32:6123–6136. https://doi.org/10.1021/acs.chemmater.0c01825
24. Randau S, Walther F, Neumann A, Schneider Y, Negi RS, Mogwitz B, Sann J, Becker-Steinberger K, Danner T, Hein S, Latz A, Richter FH, Janek J (2021) On the additive microstructure in composite cathodes and alumina-coated carbon microwires for improved all-solid-state batteries. Chem Mater 33:1380–1393. https://doi.org/10.1021/acs.chemmater.0c04454
25. Walther F, Strauss F, Wu X, Mogwitz B, Hertle J, Sann J, Rohnke M, Brezesinski T, Janek J (2021) The working principle of a Li_2CO_3/$LiNbO_3$ coating on NCM for thiophosphate-based all-solid-state batteries. Chem Mater 33:2110–2125. https://doi.org/10.1021/acs.chemmater.0c04660
26. Kitsche D, Tang Y, Ma Y, Goonetilleke D, Sann J, Walther F, Bianchini M, Janek J, Brezesinski T (2021) High performance all-solid-state batteries with a Ni-Rich NCM cathode coated by atomic layer deposition and lithium thiophosphate solid electrolyte. ACS Appl Energy Mater 4:7338–7345. https://doi.org/10.1021/acsaem.1c01487
27. Choi JH, Choi S, Embleton TJ, Ko K, Saqib KS, Ali J, Jo M, Hwang J, Park S, Kim M, Hwang M, Lim H, Oh P (2023) The effect of conductive additive morphology and crystallinity on the electrochemical performance of Ni-Rich cathodes for sulfide all-solid-state lithium-ion batteries. Nanomaterials (Basel) 13:3065. https://doi.org/10.3390/nano13233065
28. Lee KJ, Byeon YW, Lee HJ, Lee Y, Park S, Kim HR, Kim HK, Oh SJ, Ahn JP (2023) Revealing crack-healing mechanism of NCM composite cathode for sustainable cyclability of sulfide-based solid-state batteries. Energy Storage Mater 57:326–333. https://doi.org/10.1016/j.ensm.2023.01.012
29. Cangaz S, Hippauf F, Reuter FS, Doerfler S, Abendroth T, Althues H, Kaskel S (2020) Enabling high-energy solid-state batteries with stable anode interphase by the use of columnar

silicon anodes. Adv Energy Mater 10:2001320. https://doi.org/10.1002/aenm.202001320
30. Li Y, Wu Y, Ma T, Wang Z, Gao Q, Xu J, Chen L, Li H, Wu F (2022) Long-life sulfide all-solid-state battery enabled by substrate-modulated dry-process binder. Adv Energy Mater 12:2001732. https://doi.org/10.1002/aenm.202201732
31. Minnmann P, Quillman L, Burkhardt S, Richter FH, Janek J (2021) Editors' Choice—Quantifying the impact of charge transport bottlenecks in composite cathodes of all-solid-state batteries. J Electrochem Soc 168:040537. https://doi.org/10.1149/1945-7111/abf8d7
32. Ann J, Choi S, Do J, Lim S, Shin D (2018) Effects of binary conductive additives on electrochemical performance of a sheet-type composite cathode with different weight ratios of $LiNi_{0.6}Co_{0.2}Mn_{0.2}O_2$ in all-solid-state lithium batteries. J Ceram Process Res 19:413
33. Poetke S, Hippauf F, Baasner A, Dörfler S, Althues H, Kaskel S (2021) Nanostructured Si−C composites as high-capacity anode material for all-solid-state lithium-ion batteries. Batteries Supercaps 4:1323–1334. https://doi.org/10.1002/batt.202100055
34. Jun S, Nam YJ, Kwak H, Kim KT, Oh DY, Jung YS (2020) Operando differential electrochemical pressiometry for probing electrochemo-mechanics in all-solid-state batteries. Adv Funct Mater 30:2002535. https://doi.org/10.1002/adfm.202002535
35. Fang R, Liu Y, Li Y, Manthiram A, Goodenough JB (2023) Achieving stable all-solid-state lithium-metal batteries by tuning the cathode-electrolyte interface and ionic/electronic transport within the cathode. Mater Today 64:52–60. https://doi.org/10.1016/j.mattod.2023.03.001
36. Kim KT, Woo J, Kim YS, Sung S, Park C, Lee C, Park YJ, Lee HW, Park K, Jung YS (2023) Ultrathin superhydrophobic coatings for air-stable inorganic solid electrolytes: toward dry room application for all-solid-state batteries. Adv Energy Mater 13:2301600. https://doi.org/10.1002/aenm.202301600
37. Tan DHS, Wu EA, Nguyen H, Chen Z, Marple MAT, Doux JM, Wang X, Yang H, Banerjee A, Meng YS (2019) The detrimental effects of carbon additives in $Li_{10}GeP_2S_{12}$-based solid-state batteries. ACS Energy Lett 4:2418–2427. https://doi.org/10.1021/acsenergylett.9b01693
38. Zhang W, Leichtweiß T, Culver SP, Koerver R, Das D, Weber DA, Zeier WG, Janek J (2017) The detrimental effects of carbon additives in Li10GeP2S12-based solid-state batteries. ACS Appl Mater Interfaces 9:35888–35896. https://doi.org/10.1021/acsami.7b11530
39. Teo JH, Strauss F, Tripkovi Đ, Schweidler S, Ma Y, Bianchini M, Janek J, Brezesinski T (2021) Design-of-experiments-guided optimization of slurry-cast cathodes for solid-state batteries. Cell Rep Physiol Sci 2:100465. https://doi.org/10.1016/j.xcrp.2021.100465
40. Yamamoto M, Terauchi Y, Sakuda A, Takahashi M (2018) Slurry mixing for fabricating silicon-composite electrodes in all-solid-state batteries with high areal capacity and cycling stability. J Power Sources 402:506–512. https://doi.org/10.1016/j.jpowsour.2018.09.070
41. Kim AY, Strauss F, Bartsch T, Teo JH, Janek J, Brezesinski T (2021) Effect of surface carbonates on the cyclability of $LiNbO_3$-coated NCM622 in all-solid-state batteries with lithium thiophosphate electrolytes. Sci Rep 11:5367. https://doi.org/10.1038/s41598-021-84799-1
42. Embleton TJ, Yun J, Choi JH, Kim J, Ko K, Kim J, Son Y, Oh P (2023) Lithium-enhanced functionalized carbon nanofibers as a mixed electronic/ionic conductor for sulfide all solid-state batteries. Appl Surf Sci 610:155490. https://doi.org/10.1016/j.apsusc.2022.155490
43. Swamy T, Chen X, Chiang YM (2019) Electrochemical redox behavior of Li ion conducting sulfide solid electrolytes. Chem Mater 31:707–713. https://doi.org/10.1021/acs.chemmater.8b03420
44. Hakari T, Deguchi M, Mitsuhara K, Ohta T, Saito K, Orikasa Y, Uchimoto Y, Kowada Y, Hayashi A, Tatsumisago M (2017) Structural and electronic-state changes of a sulfide solid electrolyte during the Li deinsertion–insertion processes. Chem Mater 29:4768–4774. https://doi.org/10.1021/acs.chemmater.7b00551
45. Rossman RP, Smith WR (1943) Density of carbon black by helium displacement. Ind Eng Chem 35:972–976. https://doi.org/10.1021/ie50405a008
46. Bielefeld A, Weber DA, Janek J (2019) Microstructural modeling of composite cathodes for all-solid-state batteries. J Phys Chem C 123:1626–1634. https://doi.org/10.1021/acs.jpcc.8b11043
47. Ohta N, Takada K, Sakaguchi I, Zhang L, Ma R, Fukuda K, Osada M, Sasaki T (2007) $LiNbO_3$-coated $LiCoO_2$ as cathode material for all solid-state lithium secondary batteries. Electrochem Commun 9:1486–1490. https://doi.org/10.1016/j.elecom.2007.02.008
48. Gao X, Liu B, Hu B, Ning Z, Jolly DS, Zhang S, Perera J, Bu J, Liu J, Doerrer C, Darnbrough E, Armstrong D, Grant PS, Bruce PG (2022) Solid-state lithium battery cathodes operating at low pressures. Joule 6:636–646. https://doi.org/10.1016/j.joule.2022.02.008
49. Walther F, Koerver R, Fuchs T, Ohno S, Sann J, Rohnke M, Zeier WG, Janek J (2019) Visualization of the interfacial decomposition of composite cathodes in argyrodite-based all-solid-state batteries using time-of-flight secondary-ion mass spectrometry. Chem Mater 31:3745–3755. https://doi.org/10.1021/acs.chemmater.9b00770
50. Kobayashi K, Sakka Y, Suzuki TS (2016) Development of an electrochemical impedance analysis program based on the expanded measurement model. J Ceram Soc Jpn 124:943–949. https://doi.org/10.2109/jcersj2.16120
51. Koerver R, Aygün I, Leichtweiß T, Dietrich C, Zhang W, Binder JO, Hartmann P, Zeier WG, Janek J (2017) Capacity fade in solid-state batteries: Interphase formation and chemomechanical processes in nickel-rich layered oxide cathodes and lithium thiophosphate solid electrolytes. Chem Mater 29:5574–5582. https://doi.org/10.1021/acs.chemmater.7b00931
52. Tachez M, Malugani JP, Mercier R, Robert G (1984) Ionic conductivity of and phase transition in lithium thiophosphate Li_3PS_4. Solid State Ion 14:181–185. https://doi.org/10.1016/0167-2738(84)90097-3
53. Liu Z, Fu W, Payzant EA, Yu X, Wu Z, Dudney NJ, Kiggans J, Hong K, Rondinone AJ, Liang C (2013) Anomalous high ionic conductivity of nanoporous β-Li_3PS_4. J Am Chem Soc 135:975–978. https://doi.org/10.1021/ja3110895
54. Marchini F, Porcheron B, Rousse G, Albero Blanquer LA, Droguet L, Foix D, Koç T, Deschamps M, Tarascon JM (2021) The hidden side of nanoporous β-Li_3PS_4 solid electrolyte. Adv Energy Mater 11:2101111. https://doi.org/10.1002/aenm.202101111
55. Hayakawa E, Nakamura H, Ohsaki S, Watano S (2022) Characterization of solid-electrolyte/active-material composite particles with different surface morphologies for all-solid-state batteries. Adv Powder Technol 33:103470. https://doi.org/10.1016/j.apt.2022.103470
56. Hayakawa E, Nakamura H, Ohsaki S, Watano S (2022) Dry mixing of cathode composite powder for all-solid-state batteries using a high-shear mixer. Adv Powder Technol 33:103705. https://doi.org/10.1016/j.apt.2022.103705

57. Lu X, Tsai CL, Yu S, He H, Camara O, Tempel H, Liu Z, Windmüller A, Alekseev EV, Basak S, Lu L, Eichel RA, Kungl H (2022) Lithium phosphosulfide electrolytes for solid-state batteries: Part I. Funct Mater Lett 15:2240001. https://doi.org/10.1142/S179360472240001X
58. Kobayashi K, Terabe K, Sukigara T, Sakka Y (2013) Theoretical modeling of electrode impedance for an oxygen ion conductor and metallic electrode system based on the interfacial conductivity theory. Part II: Case of the limiting process by non steady-state surface diffusion. Solid State Ion 249–250:78–85. https://doi.org/10.1016/j.ssi.2013.07.022
59. Min YJ, Lee GE, Seong JY, Shin HC (2023) Advanced electrochemical analysis of all-solid-state battery electrodes using novel potential-controllable symmetric cell. Electrochim Acta 468:143154. https://doi.org/10.1016/j.electacta.2023.143154
60. Zhang J, Zheng C, Li L, Xia Y, Huang H, Gan Y, Liang C, He X, Tao X, Zhang W (2020) Unraveling the intra and intercycle interfacial evolution of Li6PS5Cl-based all-solid-state lithium batteries. Adv Energy Mater 10:1903311. https://doi.org/10.1002/aenm.201903311